

## Topologically protected optomechanically induced transparency in a one-dimensional optomechanical array

X. Z. Hao <sup>1</sup>, X. Y. Zhang <sup>1,\*</sup>, Y. H. Zhou,<sup>2</sup> C. M. Dai,<sup>3</sup> S. C. Hou,<sup>1</sup> and X. X. Yi<sup>4,†</sup>

<sup>1</sup>*Department of Physics, Dalian Maritime University, Dalian 116026, China*

<sup>2</sup>*Quantum Information Research Center, Shangrao Normal University, Shangrao 334000, China*

<sup>3</sup>*Department of Physics, Zhejiang Sci-Tech University, Hangzhou 310018, China*

<sup>4</sup>*Center for Quantum Sciences and School of Physics, Northeast Normal University, Changchun 130024, China*



(Received 21 September 2021; revised 17 November 2021; accepted 20 December 2021; published 4 January 2022)

We investigate the optomechanically induced transparency (OMIT) in an optomechanical lattice. By controlling the frequency of the external drivings in a periodic manner, the optomechanical lattice can be regarded as a Su-Schrieffer-Heeger model. By calculating the local photon density of states for the system, we investigate the response of the system to a weak probe field. In the nondeep topological nontrivial phase, we find that the system has two nondegenerate edge modes due to the finite size of the system. In this regime, a narrow transparency window of the probe field, which is much narrower than the scale set by photon decay, can be observed due to the destructive interference of the probe field absorption paths induced by the two nondegenerate edge modes. In the deep topological nontrivial phase, the two edge modes become degenerate and the narrow transparency window changes into a wide absorption window. The OMIT of the optomechanical array can also be observed in the presence of large disorders of the many-photon optomechanical couplings. Our work generalizes the OMIT of a single optomechanical cavity to a topological optomechanical system and might have potential applications in quantum information processing and quantum optical devices.

DOI: [10.1103/PhysRevA.105.013505](https://doi.org/10.1103/PhysRevA.105.013505)

### I. INTRODUCTION

Cavity optomechanical systems [1], in which optical cavities couple to mechanical oscillators via radiation pressure, have received considerable attention due to their potential applications in various aspects, e.g., high-precision measurement [2–7], exploration of the quantum-to-classical transition [8,9], and quantum information processing [10–12]. Due to the nonlinear optomechanical coupling, optomechanical systems provide a promising platform for the investigation of various quantum phenomena, such as quantum entanglement [13–18], photon and phonon blockade [19–25], ground-state cooling of mechanical oscillators [26–31], and the generation of squeezed light [32–34]. Among the various breakthroughs, a particular phenomenon which is related to our work here is optomechanically induced transparency (OMIT) [35–37], which results from the destructive interference between the anti-Stokes scattering field and the weak probe field. Recently, OMIT has also been investigated in various kind of optomechanical systems, e.g., quadratically coupled optomechanical systems [38,39], spinning optomechanical systems [40,41], non-Hermitian optomechanical systems [42,43], Laguerre-Gaussian rotational-cavity optomechanical systems [44], multimode optomechanical systems [45–47], hybrid optomechanical systems [48,49], and optomechanical lattice [50].

Over the past decades, topological systems [51–53] have attracted increasing attention and interest due to the existence of spatially localized edge states which are immune to fabrication imperfections and disorders. Topological protected edge states have been proposed and realized in a variety of systems, e.g., arrays of coupled resonators [54–57], ultracold atomic gases [58–63], helical waveguide arrays [64,65], and non-Hermitian systems [66–74]. Among the various proposed models of topological systems, the simplest one-dimensional topological model is the Su-Schrieffer-Heeger (SSH) model [75,76], which is one of the most basic topological models and provides intuitive ways to understand topological phenomena such as topological invariant, phase transition, and bulk-boundary correspondence [75–77]. Another merit of the SSH model is that it can be easily realized in various quantum systems and used to verify a variety of quantum phenomena related to topology. The SSH model can be realized in the cold atoms trapped in optical lattices [78–81], graphene ribbons [82–84], superconducting circuits [85,86], and  $p$ -orbit optical ladder systems [87]. Based on these platforms, a variety of topological properties of the SSH model have been studied, such as topological lasing [88–90], anomalous edge states [91], quantum walks [92–94], and edge state and topological phase transitions [95–97].

Recently, schemes realizing a topological SSH model in an optomechanical array have been proposed in Ref. [98–100], in which the authors have also investigated state transfer by using the edge states of the SSH model. Based on these schemes, in this paper we investigate another property of the SSH model, i.e., the response of a finite optomechanical array,

\*zhangxingyuan1@foxmail.com

†yixx@nenu.edu.cn

which can be mapped to a SSH model, to a weak probe field. We investigate the response of the optomechanical array to a weak probe field by calculating the local photon density of states (DOS) of the system. In the topological trivial phase, the local photon DOS of the system exhibits a two-band structure with a gap. In the nondeep topological nontrivial phase in which the intercell coupling is slightly larger than the intracell coupling, in addition to the two-band structure the local photon DOS has two additional narrow peaks in the gap, which correspond to the two edge modes of the system. The appearance of the two narrow peaks indicates that the two edge modes are nondegenerate and have decay rates much smaller than the photon loss. In the deep topological nontrivial phase in which the intercell coupling is much larger than the intracell coupling, the two additional narrow peaks in the gap merge into one wide peak. This is because the energy difference between the two edge modes decreases as the intercell coupling strength increases. When the energy difference between the two edge modes is smaller than the decay rates of the two edge modes, the two edge modes can be thought of as degenerate and only one peak appears in the gap of the DOS. By calculating the transmission rate of the probe field, we find that in the nondeep topological nontrivial phase a narrow transparency window, i.e., OMIT, can be observed in the middle of the two edge modes. However, in the deep topological nontrivial phase, only one broad absorption window appears. The reason for this phenomenon is that in the nondeep topological nontrivial phase, each of the two edge modes provides an absorption path for the probe field and the destructive interference of the two absorption paths results in the OMIT. In the deep topological nontrivial phase, the two edge modes become degenerate and the probe field cannot distinguish the two absorption paths. Hence, the destructive interference of the two absorption paths cannot be formed and the system exhibits only one broad absorption window. As the energy difference between the two edge modes decreases as the size of the optomechanical array increases, the OMIT can only appear for a small finite array and disappears for a large array. Due to the topology of the SSH model, OMIT with large transmissivity can also be observed even in the presence of large disorder in the intercell and intracell coupling.

The paper is organized as follows. In Sec. II, we discuss the theoretical model of the optomechanical array considered in this work. In Sec. III, we calculate the retarded Green function of the system, through which we calculate the local photon DOS of the system and the transmission rate of the probe field. In this section, we also give out the physical mechanism behind the OMIT phenomenon and discuss the dependence of the probe field transmissivity on the parameters of the system. The influence of the disorders on the OMIT is also discussed in this section. At last, we summarize our results in Sec. IV.

## II. THEORETICAL MODEL

We consider a one-dimensional optomechanical array consisting of  $N$  unit cells [see Fig. 1(a)]. Each cell contains an optical cavity and a mechanical oscillator, coupled via radiation pressure. The  $j$ th cell couples to its adjacent cell  $j + 1$  via the radiation pressure between the mechanical oscillator in cell  $j$  and the optical cavity in cell  $j + 1$ . The total Hamil-

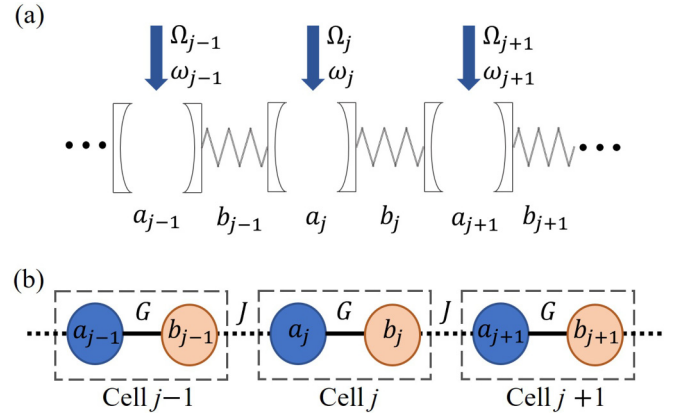


FIG. 1. (a) Schematic illustration of the one-dimensional optomechanical array. The  $j$ th cavity is driven by an external laser with the amplitude  $\Omega_j$  and the frequency  $\omega_j$ . (b) Schematic diagram of the SSH model corresponding to Hamiltonian  $\hat{H}_{\text{SSH}}$ . The intercell coupling strength between two adjacent cells is  $J$ . The intracell coupling between the optical mode and the mechanical mode in cell  $j$  is  $G$ .

tonian of the system can be written as ( $\hbar = 1$ )

$$\hat{H}_{\text{tot}} = \hat{H}_0 + \hat{H}_{\text{om}} + \hat{H}_{\text{dri}}, \quad (1)$$

with

$$\begin{aligned} \hat{H}_0 &= \sum_{j=1}^N (\omega_{a,j} \hat{a}_j^\dagger \hat{a}_j + \omega_{m,j} \hat{b}_j^\dagger \hat{b}_j), \\ \hat{H}_{\text{dri}} &= \sum_{j=1}^N (\Omega_j e^{-i\omega_j t} \hat{a}_j^\dagger + \Omega_j^* e^{i\omega_j t} \hat{a}_j), \\ \hat{H}_{\text{om}} &= - \left( \sum_{j=1}^N g_j \hat{a}_j^\dagger \hat{a}_j - \sum_{j=1}^{N-1} g_j \hat{a}_{j+1}^\dagger \hat{a}_{j+1} \right) (\hat{b}_j^\dagger + \hat{b}_j). \end{aligned}$$

Here,  $\hat{a}_j$  ( $\hat{b}_j$ ) is the annihilation operator of the optical mode (mechanical mode) in cell  $j$  with the frequency  $\omega_{a,j}$  ( $\omega_{m,j}$ ).  $\hat{H}_0$  represents the free Hamiltonian of the array.  $\hat{H}_{\text{dri}}$  describes the interaction between the optical driving fields and the system. The cavity in cell  $j$  is driven by an optical laser with the driving frequency  $\omega_j$  and the amplitude  $\Omega_j$ .  $\hat{H}_{\text{om}}$  represents the radiation pressure coupling between the optical cavities and the mechanical oscillators. The coupling strength between the  $j$ th mechanical oscillator and the two adjacent optical cavities is  $g_j$ . In the rotating frame with respect to the optical driving frequency  $\omega_j$ , the above Hamiltonian, Eq. (1), becomes

$$\begin{aligned} \hat{H}'_{\text{tot}} &= \sum_{j=1}^N (\Delta_{a,j} \hat{a}_j^\dagger \hat{a}_j + \omega_{m,j} \hat{b}_j^\dagger \hat{b}_j + \Omega_j \hat{a}_j^\dagger + \Omega_j^* \hat{a}_j) \\ &\quad - \left( \sum_{j=1}^N g_j \hat{a}_j^\dagger \hat{a}_j - \sum_{j=1}^{N-1} g_j \hat{a}_{j+1}^\dagger \hat{a}_{j+1} \right) (\hat{b}_j^\dagger + \hat{b}_j), \end{aligned}$$

where  $\Delta_{a,j} = \omega_{a,j} - \omega_j$  is the frequency detuning of the  $j$ th optical mode with respect to its driving field. Under the condition of strong optical drives, both the field amplitudes of the cavity fields and the mechanical oscillators are large

and the standard linearization process can be performed by writing  $\hat{a}_j = \alpha_j + \hat{a}_j$  and  $\hat{b}_j = \beta_j + \hat{b}_j$ , where  $\alpha_j = \langle \hat{a}_j \rangle$  and  $\beta_j = \langle \hat{b}_j \rangle$ , where  $\hat{a}_j$  and  $\hat{b}_j$  are the fluctuation operators of  $\hat{a}_j$  and  $\hat{b}_j$ , respectively. For simplification, we assume that all the mechanical oscillators have the same frequency, i.e.,  $\omega_{m,j} = \omega_m$ . The linearized Hamiltonian is given by

$$\hat{H}_{\text{lin}} = \hat{H}_{\text{RWA}} + \hat{H}_{\text{CRWA}}, \quad (2)$$

with

$$\begin{aligned} \hat{H}_{\text{RWA}} &= \sum_{j=1}^N (\Delta'_{a,j} \hat{a}_j^\dagger \hat{a}_j + \omega_m \hat{b}_j^\dagger \hat{b}_j) \\ &\quad - \sum_{j=1}^N (G_j \hat{a}_j^\dagger \hat{b}_j + G_j^* \hat{a}_j \hat{b}_j^\dagger) \\ &\quad + \sum_{j=1}^{N-1} (J_j \hat{a}_{j+1}^\dagger \hat{b}_j + J_j^* \hat{a}_{j+1} \hat{b}_j^\dagger), \\ \hat{H}_{\text{CRWA}} &= - \sum_{j=1}^N (G_j \hat{a}_j^\dagger \hat{b}_j^\dagger + G_j^* \hat{a}_j \hat{b}_j) \\ &\quad + \sum_{j=1}^{N-1} (J_j \hat{a}_{j+1}^\dagger \hat{b}_j^\dagger + J_j^* \hat{a}_{j+1} \hat{b}_j). \end{aligned}$$

The effective many-photon optomechanical couplings are  $G_j = g_j \alpha_j$  and  $J_j = g_j \alpha_{j+1}$ . The periodic modulation of the effective optomechanical couplings, i.e.,  $G_j = G$  and  $J_j = J$ , can be achieved by changing the frequencies of the optical drivings in the way of periodic control [98–102]. As the phase of  $G$  and  $J$  can be tuned freely by changing the phases of optical driving amplitude, we assume that  $G$  and  $J$  are real. The effective cavity detunings are  $\Delta'_{a,1} = \Delta_{a,1} - g_1(\beta_1^* + \beta_1)$  and  $\Delta'_{a,j \in [2,N]} = \Delta_{a,j} - g_j(\beta_j^* + \beta_j) + g_{j-1}(\beta_{j-1}^* + \beta_{j-1})$ . For simplicity, we assume  $\Delta'_{a,j} = \omega_m$ , which can be achieved by tuning  $\Delta_{a,j}$ . In this case, the term  $\hat{H}_{\text{CRWA}}$  is large detuned under the condition  $G, J \ll \omega_m$  and can be neglected safely. The condition  $\Delta'_{a,j} = \omega_m$  means that a photon of the driving field has energy that is one phonon less than a photon of the cavity. So, if a photon of the driving field is absorbed by the  $j$ th cavity, the  $j$ th cavity must absorb one phonon, which can be provided by the  $j$ th or the  $(j-1)$ th mechanical oscillator, to compensate the energy difference. In a similar way, if the  $j$ th cavity emits a photon with the frequency of the driving field, one phonon is added to the  $j$ th or the  $(j-1)$ th mechanical oscillator. It is in this way that energy is exchanged between the optical cavities and the mechanical oscillators. Hence, after dropping the counter-rotating wave terms, the linearized Hamiltonian, Eq. (2), in the rotating frame with respect to  $\hat{H}_0 = \sum_{j=1}^N (\Delta'_{a,j} \hat{a}_j^\dagger \hat{a}_j + \omega_m \hat{b}_j^\dagger \hat{b}_j)$ , reduces to

$$\hat{H}_{\text{SSH}} = -G \sum_{j=1}^N (\hat{a}_j^\dagger \hat{b}_j + \hat{a}_j \hat{b}_j^\dagger)$$

$$+ \sum_{j=1}^{N-1} J (\hat{a}_{j+1}^\dagger \hat{b}_j + \hat{a}_{j+1} \hat{b}_j^\dagger). \quad (3)$$

In this way, the system can be thought of as a periodically modulated SSH model with  $N$  unit cells, where  $G$  and  $J$  are the intracell and the intercell coupling strength, respectively [see Fig. 1(b)]. In this work, both the intracell and the intercell coupling strength are much less than  $\omega_m$  due to the rotating-wave approximation made to  $\hat{H}_{\text{lin}}$ . However, in Ref. [103] the authors have demonstrated that a SSH model with large intracell and intercell coupling can still be achieved in an optomechanical array by periodically modulating the frequency of both cavity fields and mechanical modes. In spite of this, in this work we still consider the case that  $G, J \ll \omega_m$ . It is well known that the SSH model has two distinct phases depending on the value of  $J/G$ . When  $J/G > 1$ , the system is in the topological nontrivial phase and has two edge modes which can be written formally as

$$\hat{f}_n = \sum_{j=1}^N (\psi_{n,j} \hat{a}_j + \varphi_{n,j} \hat{b}_j), \quad (4)$$

with  $n = 1$  and  $2$ .  $\hat{f}_n$  represents the annihilation operator of the  $n$ th edge mode. The population amplitudes  $\psi_{n,j}$  and  $\varphi_{n,j}$  of Eq. (4) can be obtained by diagonalizing  $\hat{H}_{\text{SSH}}$ , i.e., Eq. (3). For a small finite lattice, the two edge modes are nondegenerate and the energy difference between the two edge modes, which can be obtained by diagonalizing  $\hat{H}_{\text{SSH}}$ , can be tuned by mediating the ratio  $J/G$ . By saying that the two edge modes are nondegenerate, we mean that the energy difference between the two edge modes is larger than the damping rates of the two edge modes, so that the two edge modes can be distinguished by a weak probe field. It is the nondegeneracy of the two edge modes that results in the OMIT. In Fig. 2(a), we plot the energy difference between the two edge modes as a function of  $J/G$ . From this figure, we can see that in the nondeep topological nontrivial phase, e.g.,  $J = 1.5G$  (point A), the two edge modes are not degenerate. Although the energy difference between the two edge modes is smaller than the decay rate of the optical cavities, the two edge modes have damping rates much smaller than the photon loss rate  $\kappa$  (see below). This means that the two edge modes are phononlike and can induce OMIT. When  $J$  is much larger than  $G$ , e.g.,  $J = 2G$  (point B), the energy difference between the two edge modes is so small that they can be seen as degenerate. Figures 2(b) and 2(c) show the probability distributions of the two edge modes with  $J = 1.5G$  (point A) and  $J = 2.0G$  (point B), respectively. From this figure, we can see that, for the two edge modes, energy only populates on the optical cavities on the left boundary and populates on the mechanical oscillators on the right boundary. This means that edge modes can be excited by coupling the probe field to the cavity of the first cell and cannot be excited by coupling the probe field to the cavity of the  $N$ th cell. So in this work we investigate the response of the SSH model to a weak probe field by coupling the probe field to the cavity of the first cell.

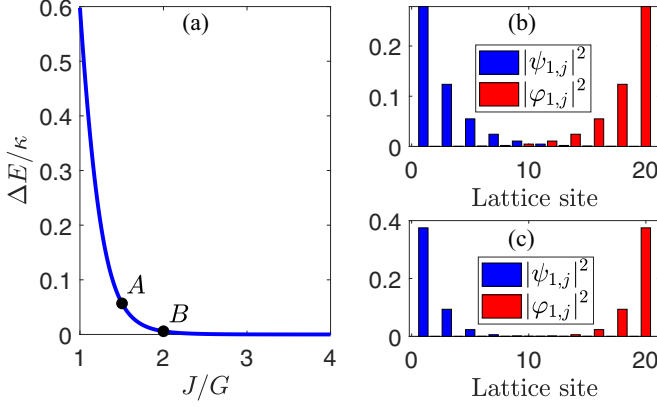


FIG. 2. (a) Energy difference between the two edge modes as a function of  $J$ . The values of the intercell coupling strength for points A and B are  $J = 1.5G$  and  $J = 2.0G$ , respectively. (b) Probability distributions of the edge modes with  $J/G = 1.5$ , i.e., point A. (c) Probability distributions of the edge modes with  $J/G = 2.0$ , i.e., point B. As the probability distributions of the two edge modes are the same, we only show the probability distribution for the first edge mode. The blue (red) bars represent the probabilities that energy populates on the optical cavities (mechanical oscillators).  $\kappa = 0.01\omega_m$  is the decay rate of the optical cavities. The intracell coupling strength is  $G = 0.02\omega_m$ . The lattice size of the system is  $N = 10$ .

### III. OMIT OF THE OPTOMECHANICAL ARRAY

#### A. Calculation of local photon DOS

In order to investigate the response of the system to a weak probe field, we follow the treatment of a one-dimensional optomechanical lattice in Ref. [50]. We first calculate the local photon DOS for an infinite optomechanical array, through which we can get the DOS of a finite array by introducing an effective potential to cut off the intercell coupling between cell  $N$  and cell  $N + 1$  and the intercell coupling between cell 0 and cell 1. The local photon DOS  $\rho(\omega, j)$  for the  $j$ th cavity of the lattice, which measures how hard it is to inject a single photon with frequency  $\omega$  to the  $j$ th cavity, is defined as

$$\rho(\omega, j) = -2\text{Im}D^R(\omega; a_j, a_j), \quad (5)$$

where  $D^R(\omega; a_j, a_j)$  is the retarded real-space Green function of cavity photons in the frequency domain.  $D^R(\omega; a_j, a_j)$  can be computed by Fourier transforming the retarded Green function in the time domain, i.e.,

$$D^R(a_j, t; a_j, t') = -i\theta(t - t')\langle[\hat{a}_j(t), \hat{a}_j^\dagger(t')]\rangle, \\ D^R(\omega; a_j, a_j) = \int_{-\infty}^{\infty} dt D^R(a_j, t; a_j, 0)e^{i\omega t}. \quad (6)$$

For an infinite array, the local photon DOS  $\rho(\omega, j)$  is not dependent on  $j$  due to the translational invariance of the system. This means that the retarded real-space Green function  $D^R(\omega, a_j, a_j)$  can be obtained by calculating the retarded Green function in  $k$  space and then transforming it back to real space. In  $k$  space, the retarded Green function of the optical modes can be obtained from the linearized Langevin equations of the system and is given by (see Appendix A for

details)

$$D^R(\omega, k) = \frac{1}{\omega - \Delta_a + i\frac{\kappa}{2} - \frac{G^2 + J^2 - 2GJ \cos k}{\omega - \omega_m + i\gamma/2}}. \quad (7)$$

By transforming the above equation to real space, the retarded real-space Green function for an infinite lattice can be written as

$$D^R(\omega; a_j, a_j) = \int_{-\pi}^{\pi} e^{ik|j-j'|} D^R(\omega, k) dk \\ = \frac{e^{iq[\omega]|j-j'|}}{2iA \sin q[\omega]}, \quad (8)$$

where  $A = \frac{GJ}{\omega - \omega_m + i\gamma/2}$  and the complex function  $q[\omega]$  satisfies

$$\omega - \Delta_a + i\frac{\kappa}{2} - \frac{G^2 + J^2 - 2GJ \cos q[\omega]}{\omega - \omega_m + i\gamma/2} = 0. \quad (9)$$

The retarded Green function for a finite lattice with  $N$  cells can be calculated by introducing an effective potential to the infinite lattice, which cuts off the interaction between cell  $N$  and cell  $N + 1$  and the coupling between cell 0 and cell 1. As we consider the situation that the waveguide couples to the cavity in cell 1, we only concern the DOS of the first cavity. The retarded Green function of the first cavity for a finite lattice can be written as (see Appendix B for details)

$$D_f^R(\omega; a_1, a_1) = \frac{(\xi e^{2iq[\omega]} - 1)(e^{(2N)iq[\omega]} - 1)}{2iA \sin q[\omega](1 - \xi e^{(2N+2)iq[\omega]}), \quad (10)$$

where  $\xi$  is defined as

$$\xi = \frac{G - J e^{-iq[\omega]}}{G - J e^{iq[\omega]}}.$$

By using Eq. (10), the local photon DOS of the first cavity can be calculated from the definition, Eq. (5), i.e.,

$$\rho(\omega, 1) = -2\text{Im}D_f^R(\omega; a_1, a_1). \quad (11)$$

Figure 3(a) shows the local photon DOS of the first cavity, i.e., Eq. (11), for different intercell coupling strength  $J$ . From this figure, we can see that when  $J/G < 1$ , which means that the SSH model is in the topological trivial phase, the local photon DOS exhibits a two-band structure, separated by a gap which is centered on  $\omega = \omega_m$ . When  $J$  is a little larger than  $G$ , i.e.,  $J = 1.2G$ , two additional narrow peaks, which indicate the appearance of the two edge modes, appear in the gap. In this case, the energy difference between the two edge modes is larger than the linewidth of the two edge modes and the two edge modes are nondegenerate. If the intercell coupling strength increases further, the energy difference between the two edge modes becomes so small that it is smaller than the linewidth of the two edge modes. The two peaks of the DOS near  $\omega = \omega_m$  merge into one peak and the two edge modes can be seen as degenerate.

#### B. OMIT of the system

In order to investigate the response of the system to a weak probe field, we assume that an additional waveguide couples to the cavity in the first cell. According to the standard input-output theory [104], the additional waveguide increases the decay rate of the first cavity from  $\kappa$  to  $\kappa + \kappa_{\text{ex},1} \equiv \kappa_1$ , where

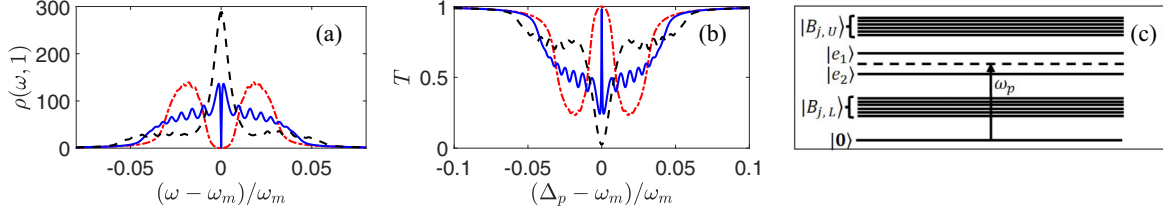


FIG. 3. (a) Local photon DOS  $\rho(\omega, 1)$  for the first cavity of the lattice with different intercell coupling  $J$ . (b) Transmission rate of the probe field as a function of the probe-control field detuning  $\Delta_p$  for different intercell coupling  $J$ . In panels (a) and (b), the intercell coupling strength is  $J = 0.6G$  (red dash-dotted line),  $J = 1.2G$  (blue solid line) and  $J = 1.9G$  (black dashed line). The decay rates of the cavities and the mechanical oscillators are  $\kappa = 0.01\omega_m$  and  $\gamma = 10^{-5}\omega_m$ , respectively. The intracell coupling strength is  $G = 0.02\omega_m$ . The lattice size is  $N = 10$ . (c) Illustration of the destructive interference in the edge mode picture.  $|0\rangle$  represents the vacuum state of the system; i.e., all the optical cavities and the mechanical oscillators are in their vacuum state.  $|e_1\rangle$  and  $|e_2\rangle$  are the states that there is one exciton in the first and second edge mode, respectively.  $|B_{j,U}\rangle$  ( $|B_{j,L}\rangle$ ) represents that there is one exciton in the  $j$ th bulk mode of the upper (lower) band of the SSH model.

$\kappa_{\text{ex},1}$  represents the coupling strength between the cavity and the probe waveguide. As the first cavity is coupled to a probe field, the noise operator for the first cavity has a nonzero average, i.e.,

$$\langle \hat{a}_{1,\text{in}}(t) \rangle = \bar{a}_{1,\text{in}} e^{-i\Delta_p t}, \quad (12)$$

where  $\Delta_p = \omega_p - \omega_1$  is the detuning between the probe field and the driving field of the first cavity.  $\bar{a}_{1,\text{in}}$  is the amplitude of the probe field. According to the standard input-output theory [104], the corresponding average output field of the first cavity can be written as

$$\hat{a}_{1,\text{out}} = \hat{a}_{1,\text{in}} + \sqrt{\kappa_{\text{ex},1}} \hat{a}_1. \quad (13)$$

By using the above equation, the transmission rate of the probe field is given by [50]

$$T = \left| \frac{\langle \hat{a}_{1,\text{out}} \rangle}{\langle \hat{a}_{1,\text{in}} \rangle} \right|^2 = |1 - i\kappa_{\text{ex},1} \tilde{D}_f^R(\Delta_p; a_1, a_1)|^2. \quad (14)$$

$\tilde{D}_f^R(\Delta_p; a_1, a_1)$  is the “dressed” Green function of the first cavity which incorporates the effects of the coupling to the probe waveguide.  $\tilde{D}_f^R(\Delta_p; a_1, a_1)$  can be calculated by introducing an extra non-Hermitian potential for the first cavity [50], i.e.,

$$\hat{V} = -i \frac{\kappa_{\text{ex},1}}{2} \hat{a}_1^\dagger \hat{a}_1. \quad (15)$$

As the physical quantity, which determines  $T$ , is  $\langle \hat{a}_1 \rangle$ , the introduction of an extra non-Hermitian potential  $\hat{V}$  is sufficient to take into account the influence of the probe waveguide on the dynamics of  $\langle \hat{a}_1 \rangle$ . By solving the Dyson equation which including this extra potential Eq. (15), the formula of  $\tilde{D}_f^R(\Delta_p; a_1, a_1)$  can be written as (see Appendix B for details)

$$\tilde{D}_f^R(\omega; a_1, a_1) = \frac{(\xi' e^{2iq[\omega]} - 1)(e^{(2N)iq[\omega]} - 1)}{2iA \sin q[\omega](1 - \xi' e^{(2N+2)iq[\omega]})}, \quad (16)$$

where  $\omega = \Delta_p$  and the formula of  $\xi'$  is given in Appendix B. In Fig. 3(b), we plot the transmission rate of the probe field as a function of  $\Delta_p$  for different intercell coupling strength  $J$ . When  $J = 0.6G$ , there is a wide transmission window at  $\Delta_p = \omega_m$ . This is because the local photon DOS of the system has a wide gap at  $\Delta_p = \omega_m$  and the system cannot absorb the probe field. When  $J$  is a little larger than  $G$ , i.e.,  $J = 1.2G$ , a narrow transmission window, the linewidth of

which is much smaller than the decay rate of the cavities, appears. The sharpness of the transmission window indicates that the transmission window demonstrates OMIT. As  $J$  increases to a large value so that the two peaks of the DOS near  $\Delta_p = \omega_m$  merge into one peak, the transmission window turns into a wide absorption window due to the large value of the local DOS near  $\Delta_p = \omega_m$ . Similar to electromagnetically induced transparency in atoms which can be explained by using dressed states [105,106], the appearance of OMIT in the system can also be explained in the same way [see Fig. 3(c)]. The nondegenerate two edge modes provide two absorption pathways for the probe field. One absorption pathway is that the probe field is absorbed by the first edge mode, i.e.,  $|0\rangle \rightarrow |e_1\rangle$ . The other absorption pathway is that the probe field is absorbed by the second edge mode, i.e.,  $|0\rangle \rightarrow |e_2\rangle$ . The destructive interference of the two absorption pathways can cancel the absorption of the probe field, which leads to the OMIT. From Fig. 3(b), we can also see that when  $J = 1.2G$ , the transmission rate  $T$  also exhibits many small wide transparency windows on both sides of the OMIT. These transparency windows are induced by the bulk modes of the SSH model [see Fig. 3(c)]. The decay rates of these bulk modes are on the same order of magnitude as  $\kappa$ , which means that the bulk modes of the system are photonlike. Hence, the transparency windows induced by these bulk modes are wide. In Fig. 4(a), we plot the transmissivity of the probe field near  $\Delta_p = \omega_m$  as a function of  $J$ . In the topological trivial phase, i.e.,  $J < G$ , although the transmission rate of the probe field is  $T = 1$ , the transmission window is wide [see Fig. 3(b)]. In the nondeep topological nontrivial phase, two nondegenerate edge modes emerge and the destructive interference of the two absorption paths for the probe field, which results in the phenomenon of OMIT, can be formed. When  $J$  is much larger than  $G$ , the two edge modes become degenerate and the destructive interference of the absorption for the probe field cannot be formed. Hence, the transmissivity of the probe field reduces to zero and OMIT disappears. This confirms our previous discussion. The phenomenon that in the topological nontrivial phase the transmission rate of the probe field decreases from 1 to 0 as the value of  $J/G$  increases means that perfect cancellation of the absorption of the probe field can be achieved only near the boundary between the topological trivial and nontrivial phases. In order to investigate the

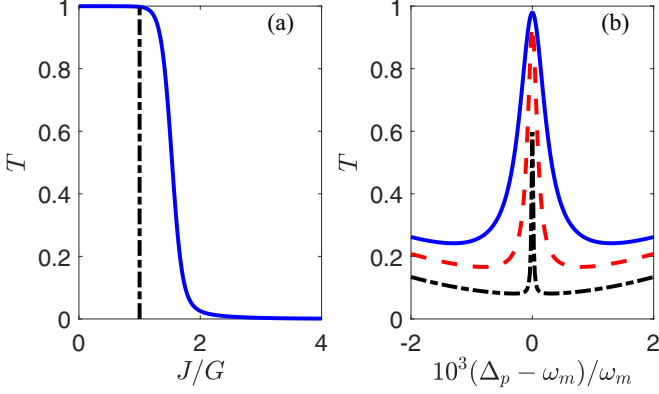


FIG. 4. (a) Transmissivity of the probe field at  $\Delta_p = \omega_m$  as a function of  $J$  (blue solid line) with the lattice size  $N = 10$ . The vertical black dash-dotted line is the boundary between the topological trivial and nontrivial phases. The region  $J/G < 1$  ( $J/G > 1$ ) is the topological trivial (nontrivial) phase. (b) Transmissivity of the probe field as a function of the probe-control field detuning  $\Delta_p$  with  $J = 1.2G$  (blue solid line),  $J = 1.3G$  (red dashed line), and  $J = 1.5G$  (black dash-dotted line). Other parameters are the same as those in Fig. 3.

dependence of the width of the transmission window on the parameter  $J/G$ , in Fig. 4(b) we plot the transmission rate of the probe field as a function of  $\Delta_p$  for different values of  $J/G$ . From this figure, we can see that the width of the transmission window decreases as the value of  $J/G$  increases. However, at the same time the transmission rate decreases as well. This means that a narrower transmission window can be obtained with the sacrifice of the transmission rate.

Figure 5(a) shows the transmissivity of the probe field as a function of the lattice size. From this figure, we can see that the transmission rate  $T$  decreases as the lattice size increases. This is because the energy difference between the two edge modes decreases as the lattice size increases. When the lattice

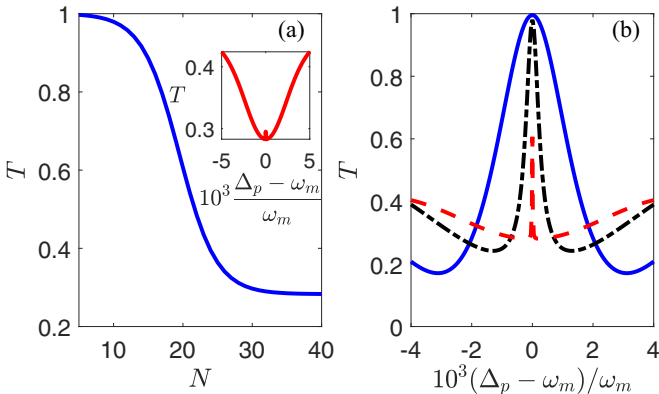


FIG. 5. (a) Transmissivity of the probe field at  $\Delta_p = \omega_m$  as a function of the lattice size  $N$ . The inset shows the transmissivity of the probe field as a function of  $\Delta_p$  with  $N = 30$ . (b) Transmissivity of the probe field as a function of  $\Delta_p$  with  $N = 6$  (blue solid line),  $N = 10$  (black dash-dotted line) and  $N = 20$  (red dashed line). The parameter  $J$  is  $J = 1.2G$ . Other parameters are the same as those in Fig. 3.

size is so large that the energy difference between the two edge modes is smaller than the damping rates of the two edge modes, the two edge modes can be seen as degenerate and the narrow transparency window becomes a wide absorption window. Indeed, when the lattice size reaches  $N = 30$ , the OMIT almost vanishes [see the inset in Fig. 5(a)]. In order to investigate the range of the lattice size under which the optomechanical array can exhibit experimentally observable OMIT, we plot the transmissivity of the probe field as a function of  $\Delta_p$  for different  $N$  in Fig. 5(b). From this figure, we can see that when the lattice size is  $N = 20$  the lattice can still have an OMIT with a transmission rate of  $T \approx 0.6$ . If the lattice size increases further, i.e.,  $N > 20$ , the transmission rate of the OMIT is small such that the OMIT may not be observable experimentally. Therefore, in order to generate experimentally observable OMIT, the lattice size should be  $N \leq 20$ . From this figure, we can also see that the width of the OMIT increases as the lattice size decreases. For the application of OMIT in quantum information processing, one wants a transparency window which is narrow and has a high transmission rate. However, from Fig. 5(b), we can see that to achieve a high transmission rate one must sacrifice the bandwidth of the transparency window. Fortunately, when the lattice size is  $N = 10$ , we can still have a narrow OMIT with a high transmission rate of  $T \approx 0.98$ . Combining the results of Figs. 4 and 5, we find that the optimal parameters, by which we can have a narrow OMIT with high transmissivity, are  $J/G = 1.2$  and  $N = 10$ .

### C. Influence of disorder

As is well known, topological systems are robust to disorder [107–111]. Now, we investigate the influence of local disorder on the OMIT of the system. We introduce disorder to the intracell and the intercell coupling strength via the Hamiltonian

$$\hat{H}_{\text{dis}} = - \sum_{j=1}^N \varepsilon_j (\hat{a}_j^\dagger \hat{b}_j + \hat{a}_j \hat{b}_j^\dagger) + \sum_{j=1}^{N-1} \zeta_j (\hat{a}_{j+1}^\dagger \hat{b}_j + \hat{a}_{j+1} \hat{b}_j^\dagger), \quad (17)$$

where  $\varepsilon_j$  and  $\zeta_j$  are random variables homogeneously distributed on  $[-\sigma, \sigma]$ ;  $\sigma$  quantifies the disorder strength. So the intercell coupling strength between cell  $j$  and cell  $j + 1$  is  $J + \zeta_j$  and the intracell coupling of the  $j$ th cell is  $G + \varepsilon_j$ . The disorder breaks the translational invariance of the SSH model. So we cannot use the method of Sec. III A to calculate the retarded Green function which determines the transmissivity of the probe field. However, we can still calculate the retarded Green function numerically. Details of the numerical method are given in Appendix C. In Fig. 6(a), we plot the transmissivity of the probe field as a function of the disorder strength. From this figure, we can see that the transmissivity of the probe field decreases first and then increases with the increase of the disorder strength. In the regime of weak disorder, i.e.,  $\sigma < G$ , the transmissivity of the probe field decreases with the increase of  $\sigma$ . In the regime of strong disorder, i.e.,  $\sigma > G$ , the transmissivity of the probe field increases with the increase

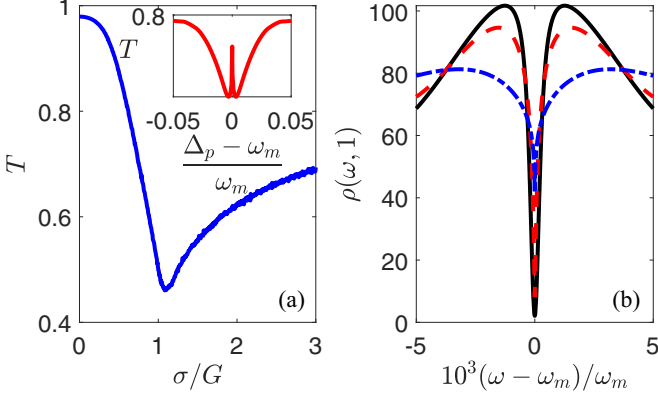


FIG. 6. (a) Transmissivity of the probe field at  $\Delta_p = \omega_m$  as a function of the disorder strength  $\sigma$ . The inset shows the transmissivity of the probe field as a function of  $\Delta_p$  with  $\sigma = 2G$ . (b) Local photon DOS  $\rho(\omega, 1)$  for the first cavity of the lattice near  $\omega = \omega_m$  with  $\sigma = 0$  (black solid line),  $\sigma = 0.4G$  (red dashed line), and  $\sigma = 2.0G$  (blue dash-dotted line). In panels (a) and (b), all the curves are obtained by taking the average over  $10^4$  disorder realizations. In panels (a) and (b), the intercell coupling strength is  $J = 1.2G$ . Other parameters are the same as those in Fig. 3.

of  $\sigma$ . In order to explain this phenomenon, in Fig. 6(b) we plot the local photon DOS  $\rho(\omega, 1)$  for the first cavity of the lattice near  $\omega = \omega_m$  with different disorder strengths. From this figure, we can see that the disorder can have two effects on the two edge modes of the system. One effect is that the disorder can broaden the two peaks of  $\rho(\omega, 1)$  near  $\omega = \omega_m$ . This means that the linewidth of the two edge modes increases as the disorder strength increases. This effect can weaken the transmissivity of the probe field. The other effect is that the two peaks of  $\rho(\omega, 1)$  move outward with the increase of the disorder strength. This means that the disorder can increase the energy difference of the two edge modes. This effect can enhance the transmissivity of the probe field. In the weak disorder regime, the first effect, i.e., the increase of bandwidth, is dominant and the transmissivity of the probe field decreases as  $\sigma$  increases. In the strong disorder regime, the second effect, i.e., the increase of the energy difference between the two edge modes, dominates and the transmissivity of the probe field increases as  $\sigma$  increases. It is the competition of the two effects that results in the nonlinear dependence of  $T$  on  $\sigma$ . Although the disorder can increase the linewidth of the two edge modes, the influence of the disorder on the linewidth of the two edge modes is small and the two edge modes are still nondegenerate for large disorder strength. Hence, OMIT with a large transmission rate can still be observed even for large disorder strength [see the inset in Fig. 6(a)].

#### IV. CONCLUSION

We have investigated the OMIT of an optomechanical array which can map to a SSH model. By calculating the transmission rate of the probe field, we find that a transparency window can be observed at  $\Delta_p = \omega_m$  in the nondeep topological nontrivial phase. The physical mechanism of this phenomenon is that in this regime the system has two nondegenerate edge modes which are phononlike. The two nondegenerate edge

modes induce two absorption paths for the probe field. Destructive interference of the two absorption paths results in the OMIT. In the deep topological nontrivial phase, the OMIT disappears because the two edge modes become degenerate. As the energy difference between the two edge modes decreases as the size of the array increases, transmissivity of the probe field decreases as the size of the array increases. When the size of the array becomes very large, the OMIT disappears. Similar to edge states of a topological system, the system can still exhibit OMIT even if the disorder of the intercell and intracell coupling is large. Our work extends the concept of OMIT to a topological system and opens up a different path to steer the performance of quantum optical devices based on OMIT.

#### ACKNOWLEDGMENTS

This work is supported by the National Natural Science Foundation of China under Grants No. 11775048 and No. 12005032 and the Fundamental Research Funds for the Central Universities under Grant No.3132021206.

#### APPENDIX A: THE RETARDED GREEN FUNCTION OF CAVITY PHOTONS IN MOMENTUM SPACE

In this Appendix, we provide a brief derivation of the  $k$ -space retarded Green function for an infinite optomechanical array under the rotating-wave approximation. The linearized Hamiltonian of an infinite lattice can be written as

$$\hat{H}_{\text{inf}} = \sum_j (\Delta_a \hat{a}_j^\dagger \hat{a}_j + \omega_m \hat{b}_j^\dagger \hat{b}_j - G \hat{a}_j^\dagger \hat{b}_j - G \hat{a}_j \hat{b}_j^\dagger + J \hat{a}_{j+1}^\dagger \hat{b}_j + J \hat{a}_{j+1} \hat{b}_j^\dagger). \quad (\text{A1})$$

Here, we have assumed that all the effective detunings of the cavities are the same, i.e.,  $\Delta'_{a,j} = \Delta_a$ . By taking the Fourier transformation  $\hat{\delta}_j = \frac{1}{\sqrt{N}} e^{ikj} \hat{\delta}_k$  ( $o = a$  and  $b$ ) to  $\hat{H}_{\text{inf}}$ , the Hamiltonian in momentum space is given by

$$\hat{H}'_{\text{inf}} = \sum_k (\Delta_a \hat{a}_k^\dagger \hat{a}_k + \omega_m \hat{b}_k^\dagger \hat{b}_k) - \sum_k (G \hat{a}_k^\dagger \hat{b}_k - J e^{-ik} \hat{a}_k^\dagger \hat{b}_k + \text{H.c.}).$$

Here,  $\hat{a}_k$  and  $\hat{b}_k$  are respectively the momentum-space photonic and phononic operators with  $k$  varying across the Brillouin zone. According to the standard input-output theory [104], the equations of motion for the photon and phonon fields can be written as

$$\begin{aligned} i \frac{\partial \hat{a}_k}{\partial t} &= \left( \Delta_a - i \frac{\kappa}{2} \right) \hat{a}_k - (G - J e^{-ik}) \hat{b}_k - i \sqrt{\kappa} \hat{a}_{k,\text{in}}, \\ i \frac{\partial \hat{b}_k}{\partial t} &= \left( \omega_m - i \frac{\gamma}{2} \right) \hat{b}_k - (G - J e^{ik}) \hat{a}_k - i \sqrt{\gamma} \hat{b}_{k,\text{in}}, \end{aligned} \quad (\text{A2})$$

where  $\hat{a}_{k,\text{in}}$  and  $\hat{b}_{k,\text{in}}$  are the noise operators of the photonic and phononic modes in momentum space, respectively. The retarded Green function in momentum space is defined as

$$\mathbf{D}^R(k; t, t') \equiv -i \theta(t - t') \langle [\hat{\psi}_k(t), \hat{\psi}_k^\dagger(t')] \rangle,$$

where  $\hat{\psi}_k = [\hat{a}_k, \hat{b}_k]^T$ . Using Eq. (A2), the equation of motions for  $\mathbf{D}^R(k; t, t')$  can be written as

$$i \frac{\partial}{\partial t} \mathbf{D}^R(k; t, t') = \mathbf{M}_k \mathbf{D}^R(k; t, t') + \delta(t - t'), \quad (\text{A3})$$

with

$$\mathbf{M}_k = \begin{pmatrix} \Delta_{a,j} - i\kappa/2 & -G + J e^{-ik} \\ -G + J e^{ik} & \omega_m - i\gamma/2 \end{pmatrix}.$$

The retarded Green function in the frequency domain can be acquired by Fourier transforming Eq. (A3), which gives

$$\mathbf{D}^R(\omega, k) = (\omega - \mathbf{M}_k)^{-1}. \quad (\text{A4})$$

The retarded Green function  $\mathbf{D}^R(\omega, k)$  is a  $2 \times 2$  matrix. The (1,1) component of Eq. (A4) represents the retarded Green function of photons in  $k$  space, i.e., Eq. (7).

## APPENDIX B: THE RETARDED GREEN FUNCTION FOR A FINITE OPTOMECHANICAL ARRAY

In this Appendix, we provide the method to calculate the retarded Green function of cavity photons for a finite optomechanical array with  $N$  cells. The retarded Green function of a finite array can be obtained from the retarded Green function of an infinite array via introducing an effective potential to cut off the coupling between cell 0 and cell 1 and the coupling between cell  $N$  and cell  $N + 1$ . In order to figure out the

formula of the effective potential, we first write out the equations satisfied by the retarded Green function of cavity photons which can be obtained by using the quantum Langevin equations corresponding to  $\hat{H}_{\text{inf}}$ . The quantum Langevin equations corresponding to  $\hat{H}_{\text{inf}}$  can be written as

$$\begin{aligned} \dot{\hat{a}}_j &= -\left(\frac{\kappa}{2} + i\Delta_a\right)\hat{a}_j + iG\hat{b}_j - iJ\hat{b}_{j-1} + \sqrt{\kappa}\hat{a}_{j,\text{in}}, \\ \dot{\hat{b}}_j &= -\left(\frac{\gamma}{2} + i\omega_m\right)\hat{b}_j + iG\hat{a}_j - iJ\hat{a}_{j+1} + \sqrt{\gamma}\hat{b}_{j,\text{in}}, \end{aligned} \quad (\text{B1})$$

where  $\kappa$  and  $\gamma$  are the decay rates of the optical cavities and the mechanical oscillators, respectively, and  $\hat{a}_{j,\text{in}}$  and  $\hat{b}_{j,\text{in}}$  are the quantum vacuum noise of the  $j$ th cavity and the thermal noise of the  $j$ th mechanical oscillator, respectively. The zero-mean-value noise operators  $\hat{a}_{j,\text{in}}$  and  $\hat{b}_{j,\text{in}}$  satisfy the commutation relations

$$[\hat{a}_{j,\text{in}}(t), \hat{a}_{j',\text{in}}^\dagger(t')] = [\hat{b}_{j,\text{in}}(t), \hat{b}_{j',\text{in}}^\dagger(t')] = \delta_{jj'}\delta(t - t')$$

and the nonzero correlation functions

$$\begin{aligned} \langle \hat{a}_{j,\text{in}}(t) \hat{a}_{j',\text{in}}^\dagger(t') \rangle &= \delta_{jj'}\delta(t - t'), \\ \langle \hat{b}_{j,\text{in}}^\dagger(t) \hat{b}_{j',\text{in}}(t') \rangle &= n_{j,\text{th}}\delta_{jj'}\delta(t - t'), \end{aligned}$$

where  $n_{j,\text{th}}$  is the mean thermal phonon number of the thermal reservoir of the  $j$ th mechanical oscillator.

In the time domain, the retarded Green functions of the system satisfy the following equations:

$$\begin{aligned} i\partial_t D^R(a_j, t; a_{j'}, t') &= i\partial_t \{-i\theta(t - t')\langle [\hat{a}_j(t), \hat{a}_{j'}^\dagger(t')] \rangle\} = \delta(t - t')\langle [\hat{a}_j(t), \hat{a}_{j'}^\dagger(t')] \rangle - i\theta(t - t')\langle [i\partial_t \hat{a}_j(t), \hat{a}_{j'}^\dagger(t')] \rangle, \\ i\partial_t D^R(b_j, t; a_{j'}, t') &= i\partial_t \{-i\theta(t - t')\langle [\hat{b}_j(t), \hat{a}_{j'}^\dagger(t')] \rangle\} = \delta(t - t')\langle [\hat{b}_j(t), \hat{a}_{j'}^\dagger(t')] \rangle - i\theta(t - t')\langle [i\partial_t \hat{b}_j(t), \hat{a}_{j'}^\dagger(t')] \rangle, \end{aligned} \quad (\text{B2})$$

where  $\theta(t - t')$  is the Heaviside function. By substituting the Langevin equations into the above equations and taking Fourier transformation for Eq. (B2), the retarded Green function defined in Eq. (6) satisfies the following coupled equations:

$$\begin{aligned} g_a(\omega)^{-1} D^R(\omega; a_j, a_{j'}) &= \delta_{jj'} - GD^R(\omega; b_j, a_{j'}) + JD^R(\omega; b_{j-1}, a_{j'}), \\ g_b(\omega)^{-1} D^R(\omega; b_j, a_{j'}) &= -GD^R(\omega; a_j, a_{j'}) + JD^R(\omega; a_{j+1}, a_{j'}), \end{aligned} \quad (\text{B3})$$

where

$$\begin{aligned} g_a(\omega)^{-1} &= \omega - \Delta_a + i\frac{\kappa}{2} + i\eta, \\ g_b(\omega)^{-1} &= \omega - \omega_m + i\frac{\gamma}{2} + i\eta. \end{aligned} \quad (\text{B4})$$

During the derivation of Eq. (B3), we have used the integral representation of the Heaviside step function, i.e.,

$$\theta(t - t') = -\frac{1}{2i\pi} \int_{-\infty}^{\infty} d\omega \frac{e^{-i\omega(t-t')}}{\omega + i\eta},$$

where  $\eta \rightarrow 0^+$  is a positive infinitesimal real number. Eliminating  $D^R(\omega; b_j, a_{j'})$ , the equation satisfied by the retarded Green function of cavity photons can be written as

$$\begin{aligned} g_a(\omega)^{-1} D^R(\omega; a_j, a_{j'}) &= \delta_{jj'} + g_b(\omega)(G^2 + J^2)D^R(\omega; a_j, a_{j'}) \\ &\quad - g_b(\omega)GJ[D^R(\omega; a_{j+1}, a_{j'}) + D^R(\omega; a_{j-1}, a_{j'})]. \end{aligned} \quad (\text{B5})$$

It should be noted that the above equation is satisfied by an infinite lattice. From Eq. (B5), the effective potential which is used to cut off the coupling between cell 0 and cell 1 is

$$\mathbf{V}_1 = \begin{pmatrix} V(0, 0) & V(0, 1) \\ V(1, 0) & V(1, 1) \end{pmatrix} = \begin{pmatrix} 0 & g_b G J \\ g_b G J & -g_b J^2 - i\frac{1}{2}k_{\text{ex},1} \end{pmatrix}.$$

The off-diagonal terms, i.e.,  $g_b G J$ , are used to cut off the coupling between cell 0 and cell 1. The term  $-g_b J^2$  in the diagonal element is used to cancel the influence of the mechanical oscillator in cell 0 on the retarded Green function of the cavity in cell 1. The term  $-i\kappa_{\text{ex},1}/2$  in the diagonal element takes into account the external decay rate due to the coupling between the cavity of cell 1 and the probe waveguide. The effective potential  $\mathbf{V}_1$  can cut the infinite lattice into a semi-infinite lattice. It should be noted that the introduction of  $\mathbf{V}_1$  (without the term  $\kappa_{\text{ex},1}$ ) is equivalent to introduce the extra term  $\hat{H}_{\text{cut},1} = -J(\hat{a}_1^\dagger \hat{b}_0 + \hat{a}_1 \hat{b}_0^\dagger)$  to the Hamiltonian of an infinite SSH model. The role of  $\hat{H}_{\text{cut},1}$  is to offset the intercell coupling between cell 0 and cell 1. The retarded Green function  $D_s^R(\omega; a_j, a_{j'})$  for a semi-infinite lattice can be obtained

from the following Dyson equation [50]:

$$\begin{pmatrix} D_s^R(\omega; a_j, a_j) & D_s^R(\omega; a_j, a_{j'}) \\ D_s^R(\omega; a_{j'}, a_j) & D_s^R(\omega; a_{j'}, a_{j'}) \end{pmatrix} - \begin{pmatrix} D^R(\omega; a_j, a_j) & D^R(\omega; a_j, a_{j'}) \\ D^R(\omega; a_{j'}, a_j) & D^R(\omega; a_{j'}, a_{j'}) \end{pmatrix} \\ = \begin{pmatrix} D^R(\omega; a_j, a_0) & D^R(\omega; a_j, a_1) \\ D^R(\omega; a_{j'}, a_0) & D^R(\omega; a_{j'}, a_1) \end{pmatrix} \begin{pmatrix} T(0, 0) & T(0, 1) \\ T(1, 0) & T(1, 1) \end{pmatrix} \begin{pmatrix} D^R(\omega; a_0, a_j) & D^R(\omega; a_0, a_{j'}) \\ D^R(\omega; a_1, a_j) & D^R(\omega; a_1, a_{j'}) \end{pmatrix}, \quad (\text{B6})$$

with

$$\begin{pmatrix} T(0, 0) & T(0, 1) \\ T(1, 0) & T(1, 1) \end{pmatrix} = \begin{pmatrix} V(0, 0) & V(0, 1) \\ V(1, 0) & V(1, 1) \end{pmatrix} \left[ 1 + \begin{pmatrix} D^R(\omega; a_0, a_0) & D^R(\omega; a_0, a_1) \\ D^R(\omega; a_1, a_0) & D^R(\omega; a_1, a_1) \end{pmatrix} \begin{pmatrix} T(0, 0) & T(0, 1) \\ T(1, 0) & T(1, 1) \end{pmatrix} \right].$$

Here,  $D^R(\omega; a_j, a_{j'})$  is the retarded Green function for an infinite lattice and is given in Eq. (8). After tedious calculations, the retarded Green function for a semi-infinite lattice can be written as

$$D_s^R(\omega; a_j, a_{j'}) = \frac{1}{2iA \sin q[\omega]} (e^{iq[\omega]|j-j'|} - e^{iq[\omega]|j+j'|} \xi'),$$

where  $q[\omega]$  is the same as defined in Eq. (9) and  $\xi'$  is defined as

$$\xi' = \frac{g_b G J - e^{-iq[\omega]} (g_b J^2 + i \frac{1}{2} k_{\text{ex},1})}{g_b G J - e^{iq[\omega]} (g_b J^2 + i \frac{1}{2} k_{\text{ex},1})}. \quad (\text{B7})$$

Following the same idea as above, the retarded Green function for the finite lattice with  $N$  cells can be calculated by introducing an effective potential, which is used to cut off the coupling between cell  $N$  and cell  $N+1$ , to the semi-infinite lattice. From Eq. (B5), the effective potential that is used to cut the coupling between cell  $N$  and cell  $N+1$  can be written as

$$\mathbf{V}_2 = \begin{pmatrix} V(N, N) & V(N, N+1) \\ V(N+1, N) & V(N+1, N+1) \end{pmatrix}, \\ = \begin{pmatrix} 0 & g_b G J \\ g_b G J & 0 \end{pmatrix}.$$

It should be noted that as the cavity in cell  $N$  does not couple to the mechanical oscillator in cell  $N+1$  directly, both the diagonal elements of  $\mathbf{V}_2$  are 0. Following the same procedure in Eq. (B6), the retarded Green function of the finite lattice is

$$\mathbf{M} = \begin{pmatrix} \frac{1}{g_a} - g_b G_1^2 & g_b G_1 J_1 & 0 & \cdots & 0 \\ g_b G_1 J_1 & \frac{1}{g_a} - g_b G_2^2 - g_b J_1^2 & g_b G_2 J_2 & \ddots & \vdots \\ 0 & \ddots & \ddots & \ddots & 0 \\ \vdots & \ddots & g_b G_{N-2} J_{N-2} & \frac{1}{g_a} - g_b G_{N-1}^2 - g_b J_{N-2}^2 & g_b G_{N-1} J_{N-1} \\ 0 & \cdots & 0 & g_b G_{N-1} J_{N-1} & \frac{1}{g_a} - g_b G_N^2 - g_b J_{N-1}^2 \end{pmatrix},$$

with

$$g'_a = \omega - \Delta_a + i \frac{\kappa_1}{2} + i\eta.$$

given by

$$D_f^R(\omega; a_j, a_{j'}) = \frac{F(\omega)}{2iA \sin q[\omega]}, \quad (\text{B8})$$

with

$$F(\omega) = \frac{(\xi' e^{2ijq[\omega]} - 1)(e^{i(2N+2-j-j')q[\omega]} - e^{i|j'-j|q[\omega]})}{(1 - \xi' e^{2i(N+1)q[\omega]})},$$

where  $\xi'$  is the same as defined in Eq. (B7). Equation (16) can be obtained from Eq. (B8) by setting  $j = j' = 1$ . By setting  $\kappa_{\text{ex},1} = 0$  and  $j = j' = 1$ , Eq. (B8) reduces to Eq. (10).

### APPENDIX C: NUMERICAL METHOD FOR THE RETARDED GREEN FUNCTION

As the waveguide is coupled to the cavity in cell 1, the retarded Green function related to the transmission rate of the probe field is  $D_f^R(\omega; a_1, a_1)$ . So the transmissivity of the probe field can be obtained by numerically simulating  $D_f^R(\omega; a_1, a_1)$ . In order to incorporate the influence of the probe waveguide on the decay rate of the cavity in cell 1, we need to change the decay rate of  $\hat{a}_1$  in Eq. (B1) from  $\kappa$  to  $\kappa_1 = \kappa + \kappa_{\text{ex},1}$ . Following the same procedure for the derivation of Eq. (B5), the closed equation satisfied by  $D_f^R(\omega; a_1, a_1)$ , for the finite lattice with  $N$  cells, is given by

$$\mathbf{M} \mathbf{D}_1 = \mathbf{N}, \quad (\text{C1})$$

where

$$\mathbf{D}_1 = [D_f^R(\omega; a_1, a_1), D_f^R(\omega; a_2, a_1), \dots, D_f^R(\omega; a_N, a_1)]^T, \\ \mathbf{N} = [1, 0, 0, \dots, 0]^T.$$

The coefficient matrix  $\mathbf{M}$  is

Here  $g_a$  and  $g_b$  are the same as defined in Eq. (B4),  $G_j$  ( $j = 1, \dots, N$ ) is the intracell coupling of the  $j$ th cell, and  $J_j$  ( $j = 1, \dots, N-1$ ) is the intercell coupling between cell  $j$  and cell  $j+1$ . The disorder of Eq. (17) can be easily added

to Eq. (C1). This can be done by setting  $G_j = G + \varepsilon_j$  and  $J_j = J + \zeta_j$ . By solving Eq. (C1) numerically, we can get the

retarded Green function  $D_f^R(\omega; a_1, a_1)$ , through which we can obtain the transmissivity of the probe field.

- 
- [1] M. Aspelmeyer, T. J. Kippenberg, and F. Marquardt, *Rev. Mod. Phys.* **86**, 1391 (2014).
- [2] X. Y. Lü, J. Q. Liao, L. Tian, and F. Nori, *Phys. Rev. A* **91**, 013834 (2015).
- [3] G. S. Agarwal and S. Huang, *Phys. Rev. A* **93**, 043844 (2016).
- [4] J. Q. Zhang, Y. Li, M. Feng, and Y. Xu, *Phys. Rev. A* **86**, 053806 (2012).
- [5] Y. He, *Appl. Phys. Lett.* **106**, 121905 (2015).
- [6] D. Y. Wang, C. H. Bai, H. F. Wang, A. D. Zhu, and S. Zhang, *Sci. Rep.* **6**, 38559 (2016).
- [7] Q. Wang, J. Q. Zhang, P. C. Ma, C. M. Yao, and M. Feng, *Phys. Rev. A* **91**, 063827 (2015).
- [8] T. J. Kippenberg and K. J. Vahala, *Science* **321**, 1172 (2008).
- [9] W. H. Zurek, *Phys. Today* **44**, 36 (1991).
- [10] K. Stannigel, P. Komar, S. J. M. Habraken, S. D. Bennett, M. D. Lukin, P. Zoller, and P. Rabl, *Phys. Rev. Lett.* **109**, 013603 (2012).
- [11] S. Rips and M. J. Hartmann, *Phys. Rev. Lett.* **110**, 120503 (2013).
- [12] X. B. Yan, W. Z. Jia, Y. Li, J. H. Wu, X. L. Li, and H. W. Mu, *Front. Phys.* **10**, 351 (2015).
- [13] J. Li, G. Li, S. Zippilli, D. Vitali, and T. Zhang, *Phys. Rev. A* **95**, 043819 (2017).
- [14] J. Q. Liao, Q. Q. Wu, and F. Nori, *Phys. Rev. A* **89**, 014302 (2014).
- [15] D. Vitali, S. Gigan, A. Ferreira, H. R. Böhm, P. Tombesi, A. Guerreiro, V. Vedral, A. Zeilinger, and M. Aspelmeyer, *Phys. Rev. Lett.* **98**, 030405 (2007).
- [16] M. J. Hartmann and M. B. Plenio, *Phys. Rev. Lett.* **101**, 200503 (2008).
- [17] R. X. Chen, L. T. Shen, Z. B. Yang, H. Z. Wu, and S. B. Zheng, *Phys. Rev. A* **89**, 023843 (2014).
- [18] S. G. Hofer, W. Wiczkorek, M. Aspelmeyer, and K. Hammerer, *Phys. Rev. A* **84**, 052327 (2011).
- [19] P. Rabl, *Phys. Rev. Lett.* **107**, 063601 (2011).
- [20] A. Nunnenkamp, K. Børkje, and S. M. Girvin, *Phys. Rev. Lett.* **107**, 063602 (2011).
- [21] J. Q. Liao and C. K. Law, *Phys. Rev. A* **87**, 043809 (2013).
- [22] X. W. Xu, A. X. Chen, and Y. X. Liu, *Phys. Rev. A* **94**, 063853 (2016).
- [23] T. Ramos, V. Sudhir, K. Stannigel, P. Zoller, and T. J. Kippenberg, *Phys. Rev. Lett.* **110**, 193602 (2013).
- [24] H. Xie, C. G. Liao, X. Shang, M. Y. Ye, and X. M. Lin, *Phys. Rev. A* **96**, 013861 (2017).
- [25] L. L. Zheng, T. S. Yin, Q. Bin, X. Y. Lü, and Y. Wu, *Phys. Rev. A* **99**, 013804 (2019).
- [26] J. D. Thompson, B. M. Zwickl, A. M. Jayich, F. Marquardt, S. M. Girvin, and J. G. Harris, *Nature (London)* **452**, 72 (2008).
- [27] S. Gigan, H. R. Böhm, M. Paternostro, F. Blaser, G. Langer, J. B. Hertzberg, K. C. Schwab, D. Bäuerle, M. Aspelmeyer, and A. Zeilinger, *Nature (London)* **444**, 67 (2006).
- [28] K. V. Keesidis, S. D. Bennett, S. Portolan, M. D. Lukin, and P. Rabl, *Phys. Rev. B* **88**, 064105 (2013).
- [29] Y. L. Liu and Y. X. Liu, *Phys. Rev. A* **96**, 023812 (2017).
- [30] I. Wilson-Rae, N. Nooshi, W. Zwerger, and T. J. Kippenberg, *Phys. Rev. Lett.* **99**, 093901 (2007).
- [31] F. Marquardt, J. P. Chen, A. A. Clerk, and S. M. Girvin, *Phys. Rev. Lett.* **99**, 093902 (2007).
- [32] D. W. C. Brooks, T. Botter, S. Schreppler, T. P. Purdy, N. Brahms, and D. M. Stamper-Kurn, *Nature (London)* **488**, 476 (2012).
- [33] A. H. Safavi-Naeini, S. Gröblacher, J. T. Hill, J. Chan, M. Aspelmeyer, and O. Painter, *Nature (London)* **500**, 185 (2013).
- [34] T. P. Purdy, P. L. Yu, R. W. Peterson, N. S. Kampel, and C. A. Regal, *Phys. Rev. X* **3**, 031012 (2013).
- [35] G. S. Agarwal and S. Huang, *Phys. Rev. A* **81**, 041803(R) (2010).
- [36] S. Weis, R. Rivière, S. Deléglise, E. Gavartin, O. Arcizet, A. Schliesser, and T. J. Kippenberg, *Science* **330**, 1520 (2010).
- [37] A. H. Safavi-Naeini, T. P. Mayer Alegre, J. Chan, M. Eichenfield, M. Winger, Q. Lin, J. T. Hill, D. E. Chang, and O. Painter, *Nature (London)* **472**, 69 (2011).
- [38] S. Huang and G. S. Agarwal, *Phys. Rev. A* **83**, 023823 (2011).
- [39] X. Y. Zhang, Y. H. Zhou, Y. Q. Guo, and X. X. Yi, *Phys. Rev. A* **98**, 053802 (2018).
- [40] H. Lü, Y. Jiang, Y. Z. Wang, and H. Jing, *Photonics Res.* **5**, 367 (2017).
- [41] I. M. Mirza, W. C. Ge, and H. Jing, *Opt. Express* **27**, 25515 (2019).
- [42] H. Lü, C. Q. Wang, L. Yang, and H. Jing, *Phys. Rev. Appl.* **10**, 014006 (2018).
- [43] X. Y. Zhang, Y. H. Zhou, Y. Q. Guo, and X. X. Yi, *Phys. Rev. A* **98**, 033832 (2018).
- [44] J. X. Peng, Z. Chen, Q. Z. Yuan, and X. L. Feng, *Phys. Rev. A* **99**, 043817 (2019).
- [45] H. Zhang, F. Saif, Y. Jiao, and H. Jing, *Opt. Express* **26**, 25199 (2018).
- [46] P. C. Ma, J. Q. Zhang, Y. Xiao, M. Feng, and Z. M. Zhang, *Phys. Rev. A* **90**, 043825 (2014).
- [47] T. X. Lu, Y. F. Jiao, H. L. Zhang, F. Saif, and H. Jing, *Phys. Rev. A* **100**, 013813 (2019).
- [48] Y. F. Jiao, T. X. Lu, and H. Jing, *Phys. Rev. A* **97**, 013843 (2018).
- [49] K. Ullah, H. Jing, and F. Saif, *Phys. Rev. A* **97**, 033812 (2018).
- [50] W. Chen and A. A. Clerk, *Phys. Rev. A* **89**, 033854 (2014).
- [51] M. Z. Hasan and C. L. Kane, *Rev. Mod. Phys.* **82**, 3045 (2010).
- [52] X. L. Qi and S. C. Zhang, *Rev. Mod. Phys.* **83**, 1057 (2011).
- [53] T. Ozawa, H. M. Price, A. Amo, N. Goldman, M. Hafezi, L. Lu, M. C. Rechtsman, D. Schuster, J. Simon, O. Zilberberg, and I. Carusotto, *Rev. Mod. Phys.* **91**, 015006 (2019).
- [54] M. Hafezi, E. A. Demler, M. D. Lukin, and J. M. Taylor, *Nat. Phys.* **7**, 907 (2011).
- [55] R. O. Umucalilar and I. Carusotto, *Phys. Rev. Lett.* **108**, 206809 (2012).
- [56] X. B. Luo, J. H. Huang, and C. H. Lee, *Phys. Rev. A* **84**, 053847 (2011).

- [57] Z. Y. Zeng, L. Li, B. Y. Yang, J. P. Xiao, and X. B. Luo, *Phys. Rev. A* **102**, 012221 (2020).
- [58] G. Jutzu, M. Messer, R. Desbuquois, M. Lebrat, T. Uehlinger, D. Greif, and T. Esslinger, *Nature (London)* **515**, 237 (2014).
- [59] B. K. Stuhl, H. I. Lu, L. M. Ayccock, D. Genkina, and I. B. Spielman, *Science* **349**, 1514 (2015).
- [60] M. Mancini, G. Pagano, G. Cappellini, L. Livi, M. Rider, J. Catani, C. Sias, P. Zoller, M. Inguscio, M. Dalmonte, and L. Fallani, *Science* **349**, 1510 (2015).
- [61] N. Goldman, J. C. Budich, and P. Zoller, *Nat. Phys.* **12**, 639 (2016).
- [62] X. B. Luo, Z. Y. Zeng, Y. Guo, B. Yang, J. P. Xiao, L. Li, C. Kong, and A. X. Chen, *Phys. Rev. A* **103**, 043315 (2021).
- [63] L. P. Li, X. B. Luo, X. Y. Lü, X. X. Yang, and Y. Wu, *Phys. Rev. A* **91**, 063804 (2015).
- [64] M. C. Rechtsman, J. M. Zeuner, Y. Plotnik, Y. Lumer, D. Podolsky, F. Dreisow, S. Nolte, M. Segev, and A. Szameit, *Nature (London)* **496**, 196 (2013).
- [65] M. A. Bandres, M. C. Rechtsman, and M. Segev, *Phys. Rev. X* **6**, 011016 (2016).
- [66] Z. P. Gong, Y. Ashida, K. Kawabata, K. Takasan, S. Higashikawa, and M. Ueda, *Phys. Rev. X* **8**, 031079 (2018).
- [67] F. Song, S. Y. Yao, and Z. Wang, *Phys. Rev. Lett.* **123**, 170401 (2019).
- [68] K. Kawabata, K. Shiozaki, M. Ueda, and M. Sato, *Phys. Rev. X* **9**, 041015 (2019).
- [69] W. W. Zhu, W. X. Teo, L. H. Li, and J. B. Gong, *Phys. Rev. B* **103**, 195414 (2021).
- [70] H. C. Wu, L. Jin, and Z. Song, *Phys. Rev. B* **103**, 235110 (2021).
- [71] H. S. Xu and L. Jin, *Phys. Rev. A* **104**, 012218 (2021).
- [72] H. C. Wu, X. M. Yang, L. Jin, and Z. Song, *Phys. Rev. B* **102**, 161101(R) (2020).
- [73] H. C. Wu, L. Jin, and Z. Song, *Phys. Rev. B* **102**, 035145 (2020).
- [74] P. Wang, L. Jin, and Z. Song, *Phys. Rev. A* **99**, 062112 (2019).
- [75] W. P. Su, J. R. Schrieffer, and A. J. Heeger, *Phys. Rev. Lett.* **42**, 1698 (1979).
- [76] H. Takayama, Y. R. Lin-Liu, and K. Maki, *Phys. Rev. B* **21**, 2388 (1980).
- [77] J. K. Asbóth, L. Oroszlány, and A. Pályi, *A Short Course on Topological Insulators* (Springer, Cham, Switzerland, 2016).
- [78] E. J. Meier, F. A. An, and B. Gadway, *Nat. Commun.* **7**, 13986 (2016).
- [79] S. Ganeshan, K. Sun, and S. Das Sarma, *Phys. Rev. Lett.* **110**, 180403 (2013).
- [80] L. Li, Z. Xu, and S. Chen, *Phys. Rev. B* **89**, 085111 (2014).
- [81] D. W. Zhang, Y. Q. Zhu, Y. Zhao, H. Yan, and S. L. Zhu, *Adv. Phys.* **67**, 253 (2018).
- [82] O. Gröning, S. Wang, X. Yao, C. A. Pignedoli, G. B. Barin, C. Daniels, A. Cupo, V. Meunier, X. Feng, A. Narita, K. Müllen, P. Ruffieux, and R. Fasel, *Nature (London)* **560**, 209 (2018).
- [83] T. Cao, F. Zhao, and S. G. Louie, *Phys. Rev. Lett.* **119**, 076401 (2017).
- [84] P. Delpierre, D. Ullmo, and G. Montambaux, *Phys. Rev. B* **84**, 195452 (2011).
- [85] G. Engelhardt, M. Benito, G. Platero, and T. Brandes, *Phys. Rev. Lett.* **118**, 197702 (2017).
- [86] F. Mei, J. B. You, W. Nie, R. Fazio, S. L. Zhu, and L. C. Kwek, *Phys. Rev. A* **92**, 041805(R) (2015).
- [87] X. Li, E. Zhao, and W. Vincent Liu, *Nat. Commun.* **4**, 1523 (2013).
- [88] P. St-Jean, V. Goblot, E. Galopin, A. Lemaitre, T. Ozawa, L. Le Gratiet, I. Sagnes, J. Bloch, and A. Amo, *Nat. Photonics* **11**, 651 (2017).
- [89] M. Parto, S. Wittek, H. Hodaei, G. Harari, M. A. Bandres, J. Ren, M. C. Rechtsman, M. Segev, D. N. Christodoulides, and M. Khajavikhan, *Phys. Rev. Lett.* **120**, 113901 (2018).
- [90] H. Zhao, P. Miao, M. H. Teimourpour, S. Malzard, R. El-Ganainy, H. Schomerus, and L. Feng, *Nat. Commun.* **9**, 981 (2018).
- [91] T. Lee, *Phys. Rev. Lett.* **116**, 133903 (2016).
- [92] T. Kitagawa, M. S. Rudner, E. Berg, and E. Demler, *Phys. Rev. A* **82**, 033429 (2010).
- [93] J. K. Asboth and H. Obuse, *Phys. Rev. B* **88**, 121406(R) (2013).
- [94] M. Ezawa, *Phys. Rev. B* **100**, 165419 (2019).
- [95] F. Grusdt, M. Höning, and M. Fleischhauer, *Phys. Rev. Lett.* **110**, 260405 (2013).
- [96] S. Y. Yao and Z. Wang, *Phys. Rev. Lett.* **121**, 086803 (2018).
- [97] M. Di Liberto, A. Recati, I. Carusotto, and C. Menotti, *Phys. Rev. A* **94**, 062704 (2016).
- [98] C. H. Bai, D. Y. Wang, S. Zhang, S. T. Liu, and H. F. Wang, *Phys. Rev. A* **101**, 053836 (2020).
- [99] J. Cao, W. X. Cui, X. X. Yi, and H. F. Wang, *Phys. Rev. A* **103**, 023504 (2021).
- [100] L. Qi, G. L. Wang, S. T. Liu, S. Zhang, and H. F. Wang, *Front. Phys.* **16**, 12503 (2021).
- [101] A. Mari and J. Eisert, *Phys. Rev. Lett.* **103**, 213603 (2009).
- [102] L. Qi, Y. Xing, H. F. Wang, A. D. Zhu, and S. Zhang, *Opt. Express* **25**, 17948 (2017).
- [103] L. Qi, Y. Xing, S. T. Liu, S. Zhang, and H. F. Wang, *Phys. Rev. A* **101**, 052325 (2020).
- [104] A. A. Clerk, M. H. Devoret, S. M. Girvin, F. Marquardt, and R. J. Schoelkopf, *Rev. Mod. Phys.* **82**, 1155 (2010).
- [105] P. Anisimov and O. Kocharovskaya, *J. Mod. Opt.* **55**, 3159 (2008).
- [106] J. P. Marangos, *J. Mod. Opt.* **45**, 471 (1998).
- [107] B. Pérez-González, M. Bello, Á. Gómez-León, and G. Platero, *Phys. Rev. B* **99**, 035146 (2019).
- [108] J. C. Budich and E. J. Bergholtz, *Phys. Rev. Lett.* **125**, 180403 (2020).
- [109] C. C. Wanjura, M. Brunelli, and A. Nunnenkamp, *Phys. Rev. Lett.* **127**, 213601 (2021).
- [110] M. Scollon and M. P. Kennett, *Phys. Rev. B* **101**, 144204 (2020).
- [111] C. M. Dai, W. Wang, and X. X. Yi, *Phys. Rev. A* **99**, 033844 (2019).